ChemComm
Chemical Communications

Accepted Manuscript

This article can be cited before page numbers have been issued, to do this please use: T. Xue, S. R. Bongu, H. Hao, W. Liang, Y. Wang, F. Zhang, Z. Liu, Y. Zhang, H. Zhang and X. Cui, *Chem. Commun.*, 2020, DOI: 10.1039/D0CC01004A.

ROYAL SOCIETY OF CHEMISTRY

rsc.li/chemcomm

View Article Online
DOI: 10.1039/D0CC01004A

COMMUNICATION

Ultrasensitive Detection of MicroRNA with a Bismuthene-enabled Fluorescence Quenching Biosensor

Received 00th January 20xx,
Accepted 00th January 20xx

DOI: 10.1039/x0xx00000x

Tianyu Xue‡[c] Sudhakara Reddy Bongu,‡[a] Hao Huang,‡[a] Weiyuan Liang,[a] Yingwei Wang,[d] Feng Zhang,[a] Zhongyuan Liu,[c] Yupeng Zhang,*[a] Han Zhang,*[a] Xiaoqiang Cui*[b]

Bismuthene, a monoelemental two-dimensional material, has shown promise in the biomedicine, electronic, and energy fields due to its high carrier mobility and stability at room temperature. However, its use in biosensing applications is restricted due to the undefined quenching mechanism for dye molecules. Herein, we develop a novel ultrathin bismuthene-based sensing platform for microRNA (miRNA)-specific detection that even discriminates single-base mismatches. The detection limit can reach 60 pM. Excitingly, the fluorescence quenching mechanism of bismuthene, ground state weakly fluorescent charge transfer, is determined via femtosecond pump-probe spectroscopy. This finding provides a proof-of-concept platform to i) fundamentally explore the quenching mechanism of bismuthene and ii) sensitively detect miRNA molecules for early cancer.

MicroRNAs (miRNAs), as a type of biomarker, are a group of short and noncoding RNAs containing 19-23 nucleotides that play a key role in the early diagnosis and monitoring of diseases.[1, 2] Several miRNA detection techniques have previously been used to provide detailed nucleic acid base information, such as real-time PCR (RT-PCR),[3] rolling circle amplification (RCA),[4] microarray-based hybridization,[5] northern blotting,[6] and fluorescence methods.[7] Of these, fluorescence spectroscopy is a rapid, simple, and real-time method.[8-10] Unfortunately, finding an ideal fluorescence quencher is notoriously difficult, as is determining the defined quenching mechanism required for ultrafast optics and molecular electronics studies. Therefore, development of robust materials and exploration of their mechanisms for miRNA detection are urgently needed.

Various two-dimensional (2D) materials have attached intense attention for biomedical, electronic, environmental, and energy applications.[11] Recently, most research on 2D materials for biosensor applications has been related to graphene,[12-15] black phosphorus (BP),[16] transition metal dichalcogenides (TMDs),[16] ternary chalcogenides,[17] and MXene materials.[18, 19] The group VA elements, called "pnictogens", represent a novel untapped area for monoelemental monolayer applications.[20-22] Although several 2D group VA materials (e.g., BP, arsenene, and antimonene) have been applied in the biomedicine and analytical chemistry fields,[23, 24] developing bismuthene nanomaterials for bio-sensing is still challenging. As the heaviest atomic weight group VA compound with strong spin-orbit coupling, bismuthene possesses excellent metallic and topological properties, such as a fast carrier mobility, outstanding biocompatibility, strong light-material interactions, and chemically and thermally stable properties, which have found potential applications in biosensors.[25-27] Key to miRNA detection with a fluorogenic probe is the quenching mechanism, including Förster resonance energy transfer (FRET)[28, 29] and charge transfer (CT).[30] Most 2D materials affect dye molecule quenching by mechanisms that remain incompletely understood. Hence, exploitation of advanced techniques to better understand the fluorescence quenching mechanism of 2D materials is greatly needed.

A 2D nanomaterial highly capable of quenching dye molecules for sensing miRNAs and determining the quenching mechanism is urgently needed. In this communication, we address this issue with bismuthene nanomaterials and elucidate the quenching mechanism using photoluminescence and optical pump-probe spectroscopy. The dramatic quenching effect of bismuthene is ascribed to the ground state weakly fluorescent CT between bismuthene and the dye molecule. Using this mechanism, bismuthene nanomaterials were used to obtain a fluorescence quencher to detect the lung cancer-associated miRNA-21 biomarker and thus provide a rapid sensitive and selective detection platform for miRNA sensing.

[a] Key Laboratory of Optoelectronic Devices and Systems of Ministry of Education and Guangdong Province, Institute of Microscale Optoelectronics, Shenzhen University, Shenzhen 518060, P. R. China. E-mail: ypzhang@szu.edu.cn, hzhang@szu.edu.cn
[b] State Key Laboratory of Automotive Simulation and Control, School of Materials Science and Engineering, Key Laboratory of Automobile Materials of MOE, Jilin University, Changchun 130012, P. R. China. E-mail: xqcui@jlu.edu.cn
[c] Center for High Pressure Science, State Key Laboratory of Metastable Materials Science and Technology, Yanshan University, Qinhuangdao 066004, P. R. China.
[d] Hunan Key Laboratory for Super-microstructure and Ultrafast Process, School of Physics and Electronics, Central South University, 932 South Lushan Road, Changsha, Hunan 410083, P. R. China

†Electronic Supplementary Information (ESI) available: Experimental details. See DOI: 10.1039/x0xx00000x

‡These authors contributed equally to this work.

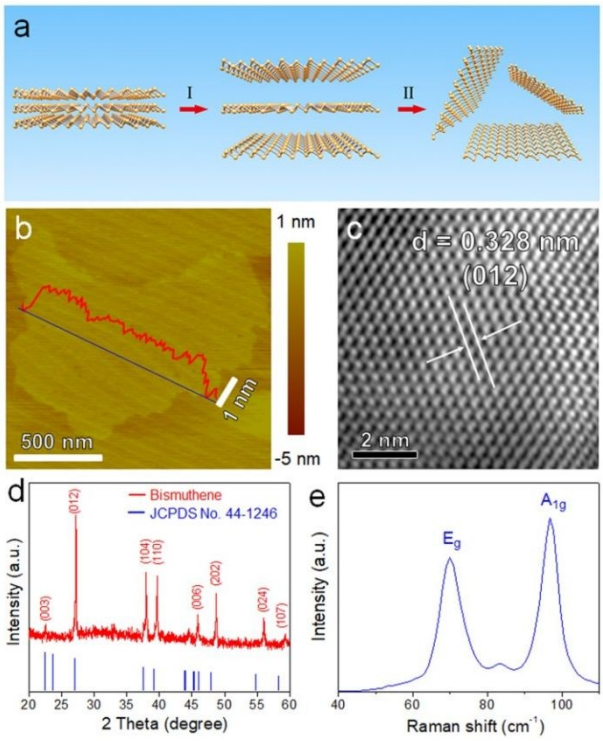

Fig. 1. Fabrication and characterization of bismuthene nanosheets. (a) Schematic depiction of the preparation process of bismuthene nanosheets. I, The bismuth solution was treated by probe sonication. II, The solution was centrifuged, and the supernatant containing bismuthene was collected. (b) AFM topography showing few-layer antimonene on mica. (c) FFT-masked HRTEM image of few-layer bismuthene nanosheets. (d) XRD spectrum of bismuthene (red line). (e) Raman spectra of few-layer bismuthene (blue line). The two peaks represent two different vibrational modes.

Liquid-phase sonication is an effective method for preparing few-layer bismuthene by breaking weak van der Waals forces. As shown in Fig. 1a, well-dispersed and ultrathin bismuthene nanosheets were successfully synthesized using probe-sonication liquid-phase exfoliation (for details, see Experimental Section). The morphology and chemical composition of the prepared samples were systematically investigated. The atomic force microscopy (AFM) topography of typical bismuthene nanosheets is shown in Fig. 1b. The overall lateral dimensions of the nanosheets are greater than 800 nm, and the thickness is approximately 1 nm, consistent with previous reports specifying the bilayer thickness of bismuthene nanosheets.[31, 32] The bismuthene structure was confirmed by high-resolution transmission electron microscopy (HRTEM). The well-resolved lattice shows its single-crystal nature, and the interlattice distance of 0.328 nm can be assigned to the (012) crystal planes of bismuthene,[33] in agreement with the X-ray diffraction (XRD) spectrum. To further investigate the crystal structure of bismuthene nanosheets, the XRD spectrum was measured as shown in Fig. 1c. The diffraction peaks of bismuthene located at 22.4°, 27.1°, 37.9°, 39.6°, 45.6°, 48.7°, 56°, and 59.3° well match the expected (003), (012), (104), (110), (006), (202), (024), and (107) planes of a Bi nanocrystal (JCPDS No. 44-1246).[34, 35] The Raman spectrum in Fig. 1e shows that the bismuthene nanosheets exhibit typical peaks at 65.6 cm^{-1} and 91 cm^{-1}, assigned as the Eg and A1g vibrational modes of bismuth, espectively.[36, 37]

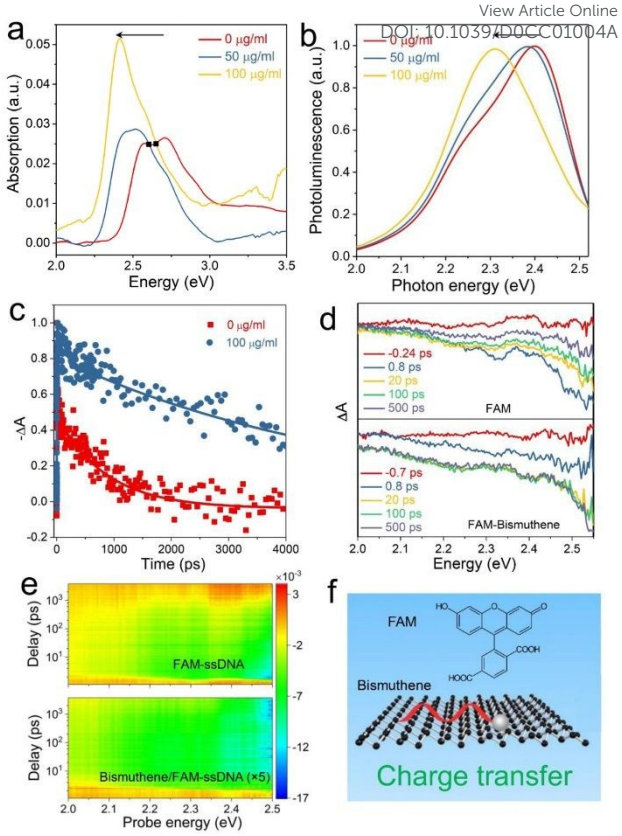

Fig. 2. (a) Linear absorption spectra of FAM-ssDNA solutions with bismuthene concentrations of 0 μg/mL (red line), 50 μg/mL (blue line), and 100 μg/mL (yellow line). (b) Typical normalized fluorescence spectra of FAM-ssDNA solutions with bismuthene concentrations of 0 μg/mL (red line), 50 μg/mL (blue line), and 100 μg/mL(yellow line). (c) Photoexcited carrier dynamics of FAM-ssDNA and bismuthene/FAM-ssDNA at a probe emission wavelength of 2.29 eV. Both decay curves were fitted with a biexponential decay function. (d) Transient absorption spectra of FAM-ssDNA and bismuthene/FAM-ssDNA at various probe delays. (e) Two-dimensional plots of the transient absorption spectra of FAM-ssDNA and bismuthene/FAM-ssDNA. (f) Schematic representation of the bismuthene/FAM-ssDNA complex.

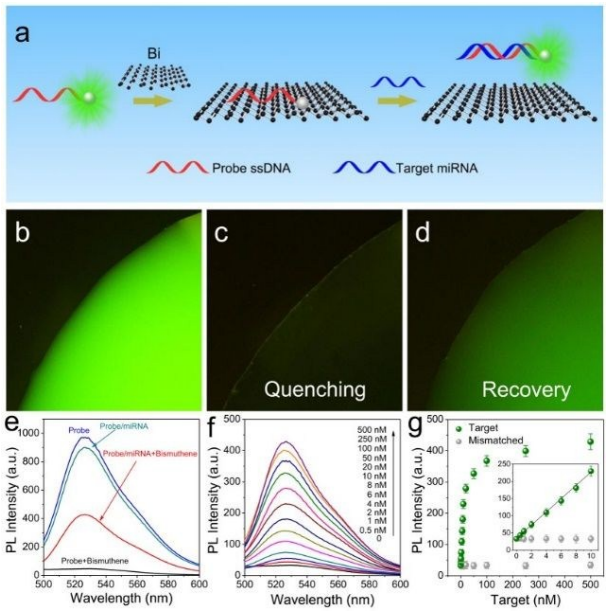

Fig. 3. (a) Schematic illustration of bismuthene nanosheet-based miRNA detection. (b) Fluorescence image of FAM-ssDNA probe solution (10^{-6} M) before mixing with bismuthene. (c) Fluorescence image of FAM-ssDNA probe solution after mixing with bismuthene. (d) Fluorescence image of FAM-ssDNA after mixing with bismuthene and incubation with miRNA-21. (e) Fluorescence spectra of the FAM-ssDNA probe (blue line), FAM-ssDNA/miRNA-21 (green line), FAM-ssDNA/miRNA-21@bismuthene (red line), and FAM-ssDNA@bismuthene (black line). (f) Fluorescence spectra of FAM-ssDNA probe solution with different concentrations of miRNA-21 and bismuthene nanosheets. (g) Relationship between the fluorescence intensity and miRNA-21/mismatched miRNA concentration. Each point corresponds to the fluorescence intensity for the indicated miRNA concentration. All error bars are the standard error of the fluorescence intensity from five data points.

To better understand the strong interaction between dye molecules and bismuthene nanosheets, fluorescein amidite (FAM), a popular fluorescein label for molecular beacons, was used to label the probe ssDNA. We carried out steady-state and time-resolved measurements. Fig. 2a shows the absorption spectra of FAM-ssDNA solutions with various concentrations of bismuthene (0, 50 μg/mL and 100 μg/mL). All the spectra were corrected to the background absorption of bismuthene. Compared to the spectrum of FAM-ssDNA, with peaks at 2.72 eV and 2.57 eV, a new band at 2.49 eV is observed after bismuthene (50 μg/mL) addition. Upon further increasing the bismuthene concentration to 100 μg/mL, the peak blueshifts further to 2.41 eV. The black dots indicated in the Fig. 2a represents the isosbestic point, where the two species in the mixture solution have the same absorption. The observation of the new absorption band along with the appearance of isosbestic points indicates the formation of a new species (FAM-ssDNA-bismuthene complex) in the system due to the ground state CT complex. Fig. 2b shows the normalized fluorescence spectra of the samples used for the absorption measurements in Fig. 2a. The FAM-ssDNA sample exhibits an emission peak at 2.40 eV. In addition to drastic suppression of the fluorescence intensity with increasing bismuthene concentration, a remarkable shift (0.09 eV) in the emission spectrum is observed, which clearly indicates the weak fluorescent nature of the CT complex.

To directly reveal the ultrafast dynamics and electron transfer of FAM-ssDNA and bismuthene, we measured the femtosecond transient absorption spectra of FAM-ssDNA and bismuthene-FAM-ssDNA complex solutions using nondegenerate pump-probe spectroscopy. Fig. 2c shows the photoexcited carrier dynamics of FAM-ssDNA and bismuthene-FAM-ssDNA at a probe emission wavelength of 2.29 eV. Compared to FAM-ssDNA (τ_1 = 3.7 ps and τ_2 = 0.86 ns), the bismuthene-FAM-ssDNA complex exhibits a considerably longer decay dynamic response (τ_1 = 30 ps and τ_2 = 5.20 ns). We compared the transient absorption spectra of FAM-ssDNA in the absence and presence of bismuthene at various probe delays (Fig. 2d). We did not observe any remarkable new bands in the transient absorption spectra of the FAM-ssDNA-bismuthene complex, indicating no evidence of an excited state interaction. Fig. 2e presents a 2D map of the transient absorption change of FAM-ssDNA in the absence and presence of bismuthene nanosheets as a function of wavelength and probe delay up to a 4 ns time window. The variation in and span of the color in the vertical direction indicate the transient absorption signal strength and dynamic response of the samples, respectively. The lower ΔA values for the FAM-ssDNA-bismuthene complex can be due to (i) the large linear absorption of bismuthene in the mixture solution[38] and (ii) quenching of the excited state within the laser pulse.[39] However, Fig. 2d and Fig. 2e clearly indicate that the complex has a considerably longer dynamic response than FAM-ssDNA over the entire wavelength range. The large dynamic response of FAM-ssDNA in the presence of bismuthene is an inherent property of the CT complex. Therefore, the energy transfer process that causes shortening of the decay dynamic response of FAM-ssDNA in the presence of bismuthene is not evident, if it even exists. Finally, we can infer that the ground state weakly fluorescent CT complex is the major contributor to the drastic suppression of the FAM-ssDNA fluorescence (Fig. 2f).

As shown in Fig. 3a, the dye-labeled ssDNA probe can be absorbed on the surface of bismuthene nanosheets via the van der Waals force between nucleobases and the basal plane of bismuthene nanosheets. We anticipated that complete fluorescent quenching of dye-labeled ssDNA on bismuthene nanosheets can occur due to bismuthene acting as a highly efficient quencher. In contrast, in the presence of the target miRNA, the formation of dsDNA weakens the interaction between the dye-labeled DNA probe and the bismuthene surface, leading to recovery fluorescence. First, to validate the feasibility of the sensing strategy mentioned above, we directly observed fluorescence images of a high concentration (10^{-6} M) solution using a fluorescence microscope. Fig. 3b depicts fluorescence microscopy images of the 10^{-6} M FAM-ssDNA probe solution. Fig. 3c shows that the fluorescence of the FAM-ssDNA probe solution is dramatically quenched once the bismuthene nanosheets are added, confirming the outstanding quenching capability of the bismuthene nanosheets. As shown in Fig. 3d, fluorescence recovery is observed under the addition of the target miRNA-21, which is primarily due to complementary binding between FAM-ssDNA and the target miRNA-21 and then desorption from bismuthene nanosheets. To further validate the observation, we performed the fluorescence spectroscopy measurement shown in Fig. 3e. The FAM-labeled ssDNA (probe) exhibits strong emission at a wavelength of 525 nm. After the addition of bismuthene nanosheets, the fluorescence of the probe is quenched to almost zero. Due to the weak interaction between dsDNA and bismuthene nanosheets, the fluorescence intensity is greatly increased to 400 with the addition of the target miRNA-21 (red curve). To confirm the sensitivity of this platform, different concentrations of miRNA-21 were hybridized with the FAM-ssDNA probe and then mixed with bismuthene nanosheets. The change in the fluorescence spectra of FAM-ssDNA upon addition of various concentrations of miRNA-21 (0 nM → 500 nm) are shown in Fig. 3f. A progressive increase in the fluoresce intensity with increasing miRNA-21 concentration is observed. To study the selectivity of this platform, a comparison of

the fluorescence recovery responses of base matched and one base mismatched miRNA-21 was performed, as shown in Fig. 3g. The response is significantly enhanced with increasing concentration of base matched miRNA-21, while no obvious variation in the response with increasing one base mismatched miRNA-21 concentration is observed. The zoomed-in view of the fluorescence recovery in Fig. 3g exhibits a linear increase with the target miRNA concentration in the range from 0 to 10 nM (inset, Fig. 3g). The detection limit is 60 pM (3 times the signal-to-noise ratio). We anticipate that bismuthene is particularly useful for intracellular experiments.[40, 41]

In conclusion, we report that bismuthene nanosheets are an effective quencher for FAM-ssDNA based on the ground state weakly fluorescent CT mechanism. Specifically, we applied this advanced material as a sensing platform to quantitatively and selectively detect miRNA. Further studies underway include intracellular experiments. Consequently, the study reveals the fluorescence quenching mechanism of bismuthene nanosheets, which is relevant to biosensor and medical applications of the material.

We acknowledge support from the National Natural Science Foundation of China (51732010, 51602305, 51702219, 61975134, 51872116), the China Postdoctoral Science Foundation (2018M633118) and the Science and Technology Innovation Commission of Shenzhen (JCYJ20180305125345378, JCYJ20170818141429525).

Conflicts of interest

There are no conflicts to declare.

Notes and references

1. G. A. Calin and C. M. Croce, *Nat. Rev. Cancer*, 2006, **6,** 857.
2. X. Chen, Y. Ba, L. Ma, X. Cai, Y. Yin, K. Wang, J. Guo, Y. Zhang, J. Chen, X. Guo, Q. Li, X. Li, W. Wang, Y. Zhang, J. Wang, X. Jiang, Y. Xiang, C. Xu, P. Zheng, J. Zhang, R. Li, H. Zhang, X. Shang, T. Gong, G. Ning, J. Wang, K. Zen, J. Zhang and C. Y. Zhang, *Cell Res.*, 2008, **18,** 997.
3. T. Thomou, M. A. Mori, J. M. Dreyfuss, M. Konishi, M. Sakaguchi, C. Wolfrum, T. N. Rao, J. N. Winnay, R. Garcia-Martin, S. K. Grinspoon, P. Gorden and C. R. Kahn, *Nature*, 2017, **542,** 450.
4. R. Deng, L. Tang, Q. Tian, Y. Wang, L. Lin and J. Li, *Angew. Chem. Int. Ed.*, 2014, **53,** 2389-2393.
5. Q. Li, B. Lowey, C. Sodroski, S. Krishnamurthy, H. Alao, H. Cha, S. Chiu, R. El-Diwany, M. G. Ghany and T. J. Liang, *Nat. Commun.*, 2017, **8,** 1789.
6. R. C. Lee and V. Ambros, *Science*, 2001, **294**, 862-864.
7. A. Qu, M. Sun, L. Xu, C. Hao, X. Wu, C. Xu, N. A. Kotov and H. Kuang, *Proc. Natl. Acad. Sci. USA*, 2019, **116**, 3391-3400.
8. S. Li, L. Xu, W. Ma, X. Wu, M. Sun, H. Kuang, L. Wang, N. A. Kotov and C. Xu, *J. Am. Chem. Soc.*, 2016, **138**, 306-312.
9. P. Zhang, X. Wu, R. Yuan and Y. Chai, *Anal. Chem.*, 2015, **87**, 3202-3207.
10. C. K. K. Choi, J. Li, K. Wei, Y. J. Xu, L. W. C. Ho, M. Zhu, K. K. W. To, C. H. J. Choi and L. Bian, *J. Am. Chem. Soc.*, 2015, **137,** 7337-7346.
11. T. Xue, S. Yu, X. Zhang, X. Zhang, L. Wang, Q. Bao, C. Chen, W. Zheng and X. Cui, *Sci. Rep.*, 2016, **6**, 21254.
12. D. Rodrigo, O. Limaj, D. Janner, D. Etezadi, F. J. García de Abajo, V. Pruneri and H. Altug, *Science*, 2015, **349**, 165-168.
13. F. Li, H. Pei, L. Wang, J. Lu, J. Gao, B. Jiang, X. Zhao and C. Fan, *Adv. Funct. Mater.*, 2013, **23**, 4140-4148.
14. T. Xue, X. Cui, W. Guan, Q. Wang, C. Liu, H. Wang, K. Qi, D. J. Singh and W. Zheng, *Biosensors Bioelectron.*, 2014, **58**, 374-379.
15. T. Xue, Z. Wang, W. Guan, C. Hou, Z. Shi, W. Zheng and X. Cui, *RSC Advances*, 2014, **4,** 50789-50794.
16. H. Liu, K. Hu, D. Yan, R. Chen, Y. Zou, H. Liu and S. Wang, *Adv. Mater.*, 2018, **30,** 1800295.
17. C. Zhu, Z. Zeng, H. Li, F. Li, C. Fan and H. Zhang, *J. Am. Chem. Soc.*, 2013, **135,** 5998-6001.
18. S. Wang, S. Wei, S. Wang, X. Zhu, C. Lei, Y. Huang, Z. Nie and S. Yao, *Anal. Chem.*, 2019, **91,** 1651-1658.
19. A. Sinha, Dhanjai, H. Zhao, Y. Huang, X. Lu, J. Chen and R. Jain, *TrAC, Trends Anal. Chem.*, 2018, **105,** 424-435.
20. C. C. Mayorga-Martinez, R. Gusmão, Z. Sofer and M. Pumera, *Angew. Chem. Int. Ed.*, 2019, **58,** 134-138.
21. S. Zhang, S. Guo, Z. Chen, Y. Wang, H. Gao, J. Gómez-Herrero, P. Ares, F. Zamora, Z. Zhu and H. Zeng, *Chem. Soc. Rev.*, 2018, **47,** 982-1021.
22. S. Zhang, Z. Yan, Y. Li, Z. Chen and H. Zeng, *Angew. Chem. Int. Ed.*, 2015, **54,** 3112-3115.
23. T. Xue, W. Liang, Y. Li, Y. Sun, Y. Xiang, Y. Zhang, Z. Dai, Y. Duo, L. Wu, K. Qi, B. N. Shivananju, L. Zhang, X. Cui, H. Zhang and Q. Bao, *Nat. Commun.*, 2019, **10,** 28.
24. J. Ji, X. Song, J. Liu, Z. Yan, C. Huo, S. Zhang, M. Su, L. Liao, W. Wang, Z. Ni, Y. Hao and H. Zeng, *Nat. Commun.*, 2016, **7,** 13352.
25. M. Pumera and Z. Sofer, *Adv. Mater.*, 2017, **29,** 1605299.
26. Y. Kadioglu, S. B. Kilic, S. Demirci, O. Ü. Aktürk, E. Aktürk and S. Ciraci, *Phys. Rev. B*, 2017, **96,** 245424.
27. Y. Wang, K. Chen, H. Hao, G. Yu, B. Zeng, H. Wang, F. Zhang, L. Wu, J. Li, S. Xiao, J. He, Y. Zhang and H. Zhang, *Nanoscale*, 2019, **11,** 2637-2643.
28. F. Federspiel, G. Froehlicher, M. Nasilowski, S. Pedetti, A. Mahmood, B. Doudin, S. Park, J.-O. Lee, D. Halley, B. Dubertret, P. Gilliot and S. Berciaud, *Nano Lett.*, 2015, **15,** 1252-1258.
29. J. J. Xu, W. W. Zhao, S. Song, C. Fan and H. Y. Chen, *Chem. Soc. Rev.*, 2014, **43,** 1601-1611.
30. Y. Xu, B. Wang, R. Kaur, M. B. Minameyer, M. Bothe, T. Drewello, D. M. Guldi and M. von Delius, *Angew. Chem.*, 2018, **130,** 11723-11727.
31. F. Reis, G. Li, L. Dudy, M. Bauernfeind, S. Glass, W. Hanke, R. Thomale, J. Schäfer and R. Claessen, *Science*, 2017, **357,** 287-290.
32. M. Zhou, W. Ming, Z. Liu, Z. Wang, P. Li and F. Liu, *Proc. Natl. Acad. Sci. USA*, 2014, **111,** 14378-14381.
33. T. Nagao, J. T. Sadowski, M. Saito, S. Yaginuma, Y. Fujikawa, T. Kogure, T. Ohno, Y. Hasegawa, S. Hasegawa and T. Sakurai, *Phys. Rev. Lett.*, 2004, **93,** 105501.
34. Y. Li, J. Wang, Z. Deng, Y. Wu, X. Sun, D. Yu and P. Yang, *J. Am. Chem. Soc.*, 2001, **123,** 9904-9905.
35. Q. Q. Yang, R. T. Liu, C. Huang, Y. F. Huang, L. F. Gao, B. Sun, Z. P. Huang, L. Zhang, C. X. Hu, Z. Q. Zhang, C. L. Sun, Q. Wang, Y. L. Tang and H. L. Zhang, *Nanoscale*, 2018, **10,** 21106-21115.
36. J. S. Lannin, J. M. Calleja and M. Cardona, *Phys. Rev. B*, 1975, **12,** 585-593.
37. Y. Wang, W. Huang, J. Zhao, H. Huang, C. Wang, F. Zhang, J. Liu, J. Li, M. Zhang and H. Zhang, *J. Mater. Chem. C*, 2019, **7,** 871-878.
38. D. Dini, M. J. F. Calvete and M. Hanack, *Chem. Rev.*, 2016, **116,** 13043-13233.
39. V. Mamidala, L. Polavarapu, J. Balapanuru, K. P. Loh, Q. H. Xu and W. Ji, *Opt. Express*, 2010, **18,** 25928-25935.
40. X. Liao, Q. Wang, H. Ju, *Chem. Commun.*, 2014, **50,** 13604-13607
41. Y. Wu, J. Huang, X. Yang, Y. Yang, K. Quan, N. Xie, J. Li, C. Ma and K. Wang, *Anal. Chem.*, 2017, **89,** 8377-8383.

View Article Online
DOI: 10.1039/D0CC01004A

COMMUNICATION

Ultrasensitive Detection of MicroRNA with a Bismuthene-enabled Fluorescence Quenching Biosensor

Received 00th January 20xx,
Accepted 00th January 20xx

DOI: 10.1039/x0xx00000x

Tianyu Xue[‡c] Sudhakara Reddy Bongu,[‡a] Hao Huang,[‡a] Weiyuan Liang,[a] Yingwei Wang,[d] Feng Zhang,[a] Zhongyuan Liu,[c] Yupeng Zhang,*[a] Han Zhang,*[a] Xiaoqiang Cui*[b]

Bismuthene, a monoelemental two-dimensional material, has shown promise in the biomedicine, electronic, and energy fields due to its high carrier mobility and stability at room temperature. However, its use in biosensing applications is restricted due to the undefined quenching mechanism for dye molecules. Herein, we develop a novel ultrathin bismuthene-based sensing platform for microRNA (miRNA)-specific detection that even discriminates single-base mismatches. The detection limit can reach 60 pM. Excitingly, the fluorescence quenching mechanism of bismuthene, ground state weakly fluorescent charge transfer, is determined via femtosecond pump-probe spectroscopy. This finding provides a proof-of-concept platform to i) fundamentally explore the quenching mechanism of bismuthene and ii) sensitively detect miRNA molecules for early cancer.

MicroRNAs (miRNAs), as a type of biomarker, are a group of short and noncoding RNAs containing 19-23 nucleotides that play a key role in the early diagnosis and monitoring of diseases.[1, 2] Several miRNA detection techniques have previously been used to provide detailed nucleic acid base information, such as real-time PCR (RT-PCR),[3] rolling circle amplification (RCA),[4] microarray-based hybridization,[5] northern blotting,[6] and fluorescence methods.[7] Of these, fluorescence spectroscopy is a rapid, simple, and real-time method.[8-10] Unfortunately, finding an ideal fluorescence quencher is notoriously difficult, as is determining the defined quenching mechanism required for ultrafast optics and molecular electronics studies. Therefore, development of robust materials and exploration of their mechanisms for miRNA detection are urgently needed.

Various two-dimensional (2D) materials have attached intense attention for biomedical, electronic, environmental, and energy applications.[11] Recently, most research on 2D materials for biosensor applications has been related to graphene,[12-15] black phosphorus (BP),[16] transition metal dichalcogenides (TMDs),[16] ternary chalcogenides,[17] and MXene materials.[18, 19] The group VA elements, called "pnictogens", represent a novel untapped area for monoelemental monolayer applications.[20-22] Although several 2D group VA materials (e.g., BP, arsenene, and antimonene) have been applied in the biomedicine and analytical chemistry fields,[23, 24] developing bismuthene nanomaterials for bio-sensing is still challenging. As the heaviest atomic weight group VA compound with strong spin-orbit coupling, bismuthene possesses excellent metallic and topological properties, such as a fast carrier mobility, outstanding biocompatibility, strong light-material interactions, and chemically and thermally stable properties, which have found potential applications in biosensors.[25-27] Key to miRNA detection with a fluorogenic probe is the quenching mechanism, including Förster resonance energy transfer (FRET)[28, 29] and charge transfer (CT).[30] Most 2D materials affect dye molecule quenching by mechanisms that remain incompletely understood. Hence, exploitation of advanced techniques to better understand the fluorescence quenching mechanism of 2D materials is greatly needed.

A 2D nanomaterial highly capable of quenching dye molecules for sensing miRNAs and determining the quenching mechanism is urgently needed. In this communication, we address this issue with bismuthene nanomaterials and elucidate the quenching mechanism using photoluminescence and optical pump-probe spectroscopy. The dramatic quenching effect of bismuthene is ascribed to the ground state weakly fluorescent CT between bismuthene and the dye molecule. Using this mechanism, bismuthene nanomaterials were used to obtain a fluorescence quencher to detect the lung cancer-associated miRNA-21 biomarker and thus provide a rapid sensitive and selective detection platform for miRNA sensing.

[a] Key Laboratory of Optoelectronic Devices and Systems of Ministry of Education and Guangdong Province, Institute of Microscale Optoelectronics, Shenzhen University, Shenzhen 518060, P. R. China. E-mail: ypzhang@szu.edu.cn, hzhang@szu.edu.cn
[b] State Key Laboratory of Automotive Simulation and Control, School of Materials Science and Engineering, Key Laboratory of Automobile Materials of MOE, Jilin University, Changchun 130012, P. R. China. E-mail: xqcui@jlu.edu.cn
[c] Center for High Pressure Science, State Key Laboratory of Metastable Materials Science and Technology, Yanshan University, Qinhuangdao 066004, P. R. China.
[d] Hunan Key Laboratory for Super-microstructure and Ultrafast Process, School of Physics and Electronics, Central South University, 932 South Lushan Road, Changsha, Hunan 410083, P. R. China

†Electronic Supplementary Information (ESI) available: Experimental details. See DOI: 10.1039/x0xx00000x

‡These authors contributed equally to this work.

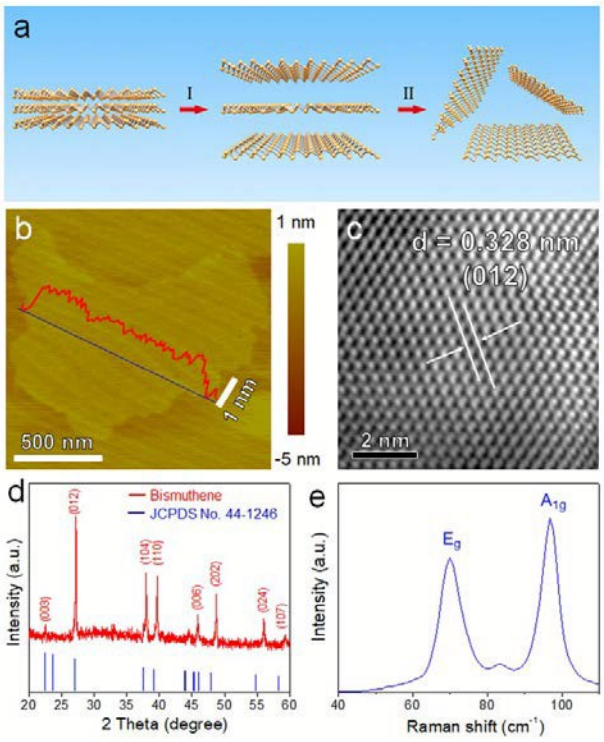

Fig. 1. Fabrication and characterization of bismuthene nanosheets. (a) Schematic depiction of the preparation process of bismuthene nanosheets. I, The bismuth solution was treated by probe sonication. II, The solution was centrifuged, and the supernatant containing bismuthene was collected. (b) AFM topography showing few-layer antimonene on mica. (c) FFT-masked HRTEM image of few-layer bismuthene nanosheets. (d) XRD spectrum of bismuthene (red line). (e) Raman spectra of few-layer bismuthene (blue line). The two peaks represent two different vibrational modes.

Liquid-phase sonication is an effective method for preparing few-layer bismuthene by breaking weak van der Waals forces. As shown in Fig. 1a, well-dispersed and ultrathin bismuthene nanosheets were successfully synthesized using probe-sonication liquid-phase exfoliation (for details, see Experimental Section). The morphology and chemical composition of the prepared samples were systematically investigated. The atomic force microscopy (AFM) topography of typical bismuthene nanosheets is shown in Fig. 1b. The overall lateral dimensions of the nanosheets are greater than 800 nm, and the thickness is approximately 1 nm, consistent with previous reports specifying the bilayer thickness of bismuthene nanosheets.[31, 32] The bismuthene structure was confirmed by high-resolution transmission electron microscopy (HRTEM). The well-resolved lattice shows its single-crystal nature, and the interlattice distance of 0.328 nm can be assigned to the (012) crystal planes of bismuthene,[33] in agreement with the X-ray diffraction (XRD) spectrum. To further investigate the crystal structure of bismuthene nanosheets, the XRD spectrum was measured as shown in Fig. 1c. The diffraction peaks of bismuthene located at 22.4°, 27.1°, 37.9°, 39.6°, 45.6°, 48.7°, 56°, and 59.3° well match the expected (003), (012), (104), (110), (006), (202), (024), and (107) planes of a Bi nanocrystal (JCPDS No. 44-1246).[34, 35] The Raman spectrum in Fig. 1e shows that the bismuthene nanosheets exhibit typical peaks at 65.6

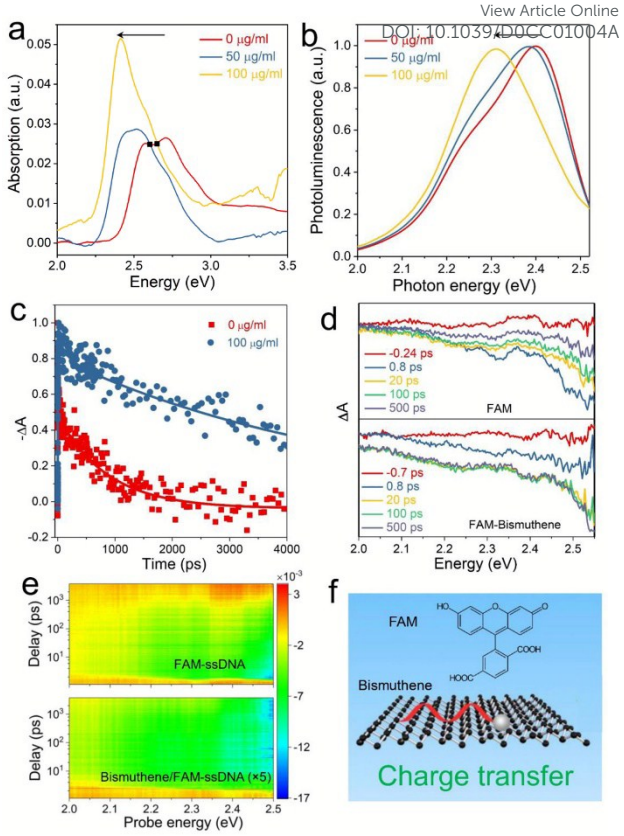

Fig. 2. (a) Linear absorption spectra of FAM-ssDNA solutions with bismuthene concentrations of 0 μg/mL (red line), 50 μg/mL (blue line), and 100 μg/mL (yellow line). (b) Typical normalized fluorescence spectra of FAM-ssDNA solutions with bismuthene concentrations of 0 μg/mL (red line), 50 μg/mL (blue line), and 100 μg/mL(yellow line). (c) Photoexcited carrier dynamics of FAM-ssDNA and bismuthene/FAM-ssDNA at a probe emission wavelength of 2.29 eV. Both decay curves were fitted with a biexponential decay function. (d) Transient absorption spectra of FAM-ssDNA and bismuthene/FAM-ssDNA at various probe delays. (e) Two-dimensional plots of the transient absorption spectra of FAM-ssDNA and bismuthene/FAM-ssDNA. (f) Schematic representation of the bismuthene/FAM-ssDNA complex.

cm^{-1} and 91 cm^{-1}, assigned as the Eg and A1g vibrational modes of bismuth, espectively.[36, 37]

To better understand the strong interaction between dye molecules and bismuthene nanosheets, fluorescein amidite (FAM), a popular fluorescein label for molecular beacons, was used to label the probe ssDNA. We carried out steady-state and time-resolved measurements. Fig. 2a shows the absorption spectra of FAM-ssDNA solutions with various concentrations of bismuthene (0, 50 μg/mL and 100 μg/mL). All the spectra were corrected to the background absorption of bismuthene. Compared to the spectrum of FAM-ssDNA, with peaks at 2.72 eV and 2.57 eV, a new band at 2.49 eV is observed after bismuthene (50 μg/mL) addition. Upon further increasing the bismuthene concentration to 100 μg/mL, the peak blueshifts further to 2.41 eV. The black dots indicated in the Fig. 2a represents the isosbestic point, where the two species in the mixture solution have the same absorption. The observation of the new absorption band along with the appearance of isosbestic points indicates the formation of a new species (FAM-ssDNA-bismuthene complex) in the system due to the ground state CT complex. Fig. 2b shows the normalized fluorescence spectra of the samples used for the absorption measurements in Fig. 2a. The FAM-ssDNA sample

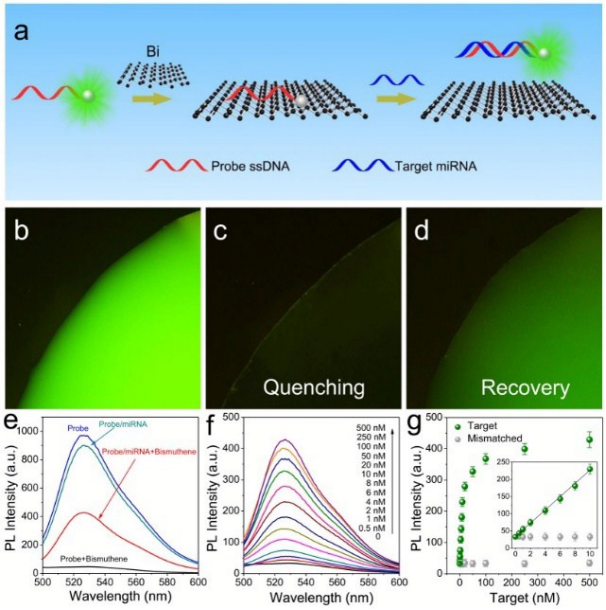

Fig. 3. (a) Schematic illustration of bismuthene nanosheet-based miRNA detection. (b) Fluorescence image of FAM-ssDNA probe solution (10^{-6} M) before mixing with bismuthene. (c) Fluorescence image of FAM-ssDNA probe solution after mixing with bismuthene. (d) Fluorescence image of FAM-ssDNA after mixing with bismuthene and incubation with miRNA-21. (e) Fluorescence spectra of the FAM-ssDNA probe (blue line), FAM-ssDNA/miRNA-21 (green line), FAM-ssDNA/miRNA-21@bismuthene (red line), and FAM-ssDNA@bismuthene (black line). (f) Fluorescence spectra of FAM-ssDNA probe solution with different concentrations of miRNA-21 and bismuthene nanosheets. (g) Relationship between the fluorescence intensity and miRNA-21/mismatched miRNA concentration. Each point corresponds to the fluorescence intensity for the indicated miRNA concentration. All error bars are the standard error of the fluorescence intensity from five data points.

exhibits an emission peak at 2.40 eV. In addition to drastic suppression of the fluorescence intensity with increasing bismuthene concentration, a remarkable shift (0.09 eV) in the emission spectrum is observed, which clearly indicates the weak fluorescent nature of the CT complex.

To directly reveal the ultrafast dynamics and electron transfer of FAM-ssDNA and bismuthene, we measured the femtosecond transient absorption spectra of FAM-ssDNA and bismuthene-FAM-ssDNA complex solutions using nondegenerate pump-probe spectroscopy. Fig. 2c shows the photoexcited carrier dynamics of FAM-ssDNA and bismuthene-FAM-ssDNA at a probe emission wavelength of 2.29 eV. Compared to FAM-ssDNA (τ_1 = 3.7 ps and τ_2 = 0.86 ns), the bismuthene-FAM-ssDNA complex exhibits a considerably longer decay dynamic response (τ_1 = 30 ps and τ_2 = 5.20 ns). We compared the transient absorption spectra of FAM-ssDNA in the absence and presence of bismuthene at various probe delays (Fig. 2d). We did not observe any remarkable new bands in the transient absorption spectra of the FAM-ssDNA-bismuthene complex, indicating no evidence of an excited state interaction. Fig. 2e presents a 2D map of the transient absorption change of FAM-ssDNA in the absence and presence of bismuthene nanosheets as a function of wavelength and probe delay up to a 4 ns time window. The variation in and span of the color in the vertical direction indicate the transient absorption signal strength and dynamic response of the samples, respectively. The lower ΔA values for the FAM-ssDNA-bismuthene complex can be due to (i) the large linear absorption of bismuthene in the mixture solution[38] and (ii) quenching of the excited state within the laser pulse.[39] However, Fig. 2d and Fig. 2e clearly indicate that the complex has a considerably longer dynamic response than FAM-ssDNA over the entire wavelength range. The large dynamic response of FAM-ssDNA in the presence of bismuthene is an inherent property of the CT complex. Therefore, the energy transfer process that causes shortening of the decay dynamic response of FAM-ssDNA in the presence of bismuthene is not evident, if it even exists. Finally, we can infer that the ground state weakly fluorescent CT complex is the major contributor to the drastic suppression of the FAM-ssDNA fluorescence (Fig. 2f).

As shown in Fig. 3a, the dye-labeled ssDNA probe can be absorbed on the surface of bismuthene nanosheets via the van der Waals force between nucleobases and the basal plane of bismuthene nanosheets. We anticipated that complete fluorescent quenching of dye-labeled ssDNA on bismuthene nanosheets can occur due to bismuthene acting as a highly efficient quencher. In contrast, in the presence of the target miRNA, the formation of dsDNA weakens the interaction between the dye-labeled DNA probe and the bismuthene surface, leading to recovery fluorescence. First, to validate the feasibility of the sensing strategy mentioned above, we directly observed fluorescence images of a high concentration (10^{-6} M) solution using a fluorescence microscope. Fig. 3b depicts fluorescence microscopy images of the 10^{-6} M FAM-ssDNA probe solution. Fig. 3c shows that the fluorescence of the FAM-ssDNA probe solution is dramatically quenched once the bismuthene nanosheets are added, confirming the outstanding quenching capability of the bismuthene nanosheets. As shown in Fig. 3d, fluorescence recovery is observed under the addition of the target miRNA-21, which is primarily due to complementary binding between FAM-ssDNA and the target miRNA-21 and then desorption from bismuthene nanosheets. To further validate the observation, we performed the fluorescence spectroscopy measurement shown in Fig. 3e. The FAM-labeled ssDNA (probe) exhibits strong emission at a wavelength of 525 nm. After the addition of bismuthene nanosheets, the fluorescence of the probe is quenched to almost zero. Due to the weak interaction between dsDNA and bismuthene nanosheets, the fluorescence intensity is greatly increased to 400 with the addition of the target miRNA-21 (red curve). To confirm the sensitivity of this platform, different concentrations of miRNA-21 were hybridized with the FAM-ssDNA probe and then mixed with bismuthene nanosheets. The change in the fluorescence spectra of FAM-ssDNA upon addition of various concentrations of miRNA-21 (0 nM → 500 nm) are shown in Fig. 3f. A progressive increase in the fluoresce intensity with increasing miRNA-21 concentration is observed. To study the selectivity of this platform, a comparison of the fluorescence recovery responses of base matched and one base mismatched miRNA-21 was performed, as shown in Fig. 3g. The response is significantly enhanced with increasing concentration of base matched miRNA-21, while no obvious variation in the response with increasing one base mismatched miRNA-21 concentration is observed. The zoomed-in view of the fluorescence recovery in Fig. 3g exhibits a linear increase with the target miRNA concentration in the range from 0 to 10 nM (inset, Fig. 3g). The detection limit is 60 pM (3 times the signal-to-noise ratio). We anticipate that bismuthene is particularly useful for intracellular experiments.[40, 41]

In conclusion, we report that bismuthene nanosheets are an effective quencher for FAM-ssDNA based on the ground state weakly fluorescent CT mechanism. Specifically, we applied this advanced material as a sensing platform to quantitatively and selectively detect miRNA. Further studies underway include intracellular experiments. Consequently, the study reveals the fluorescence quenching mechanism of bismuthene nanosheets,

which is relevant to biosensor and medical applications of the material.

We acknowledge support from the National Natural Science Foundation of China (51732010, 51602305, 51702219, 61975134, 51872116), the China Postdoctoral Science Foundation (2018M633118) and the Science and Technology Innovation Commission of Shenzhen (JCYJ20180305125345378, JCYJ20170818141429525).

Conflicts of interest

There are no conflicts to declare.

Notes and references

1. G. A. Calin and C. M. Croce, *Nat. Rev. Cancer*, 2006, **6,** 857.
2. X. Chen, Y. Ba, L. Ma, X. Cai, Y. Yin, K. Wang, J. Guo, Y. Zhang, J. Chen, X. Guo, Q. Li, X. Li, W. Wang, Y. Zhang, J. Wang, X. Jiang, Y. Xiang, C. Xu, P. Zheng, J. Zhang, R. Li, H. Zhang, X. Shang, T. Gong, G. Ning, J. Wang, K. Zen, J. Zhang and C. Y. Zhang, *Cell Res.*, 2008, **18,** 997.
3. T. Thomou, M. A. Mori, J. M. Dreyfuss, M. Konishi, M. Sakaguchi, C. Wolfrum, T. N. Rao, J. N. Winnay, R. Garcia-Martin, S. K. Grinspoon, P. Gorden and C. R. Kahn, *Nature*, 2017, **542,** 450.
4. R. Deng, L. Tang, Q. Tian, Y. Wang, L. Lin and J. Li, *Angew. Chem. Int. Ed.*, 2014, **53,** 2389-2393.
5. Q. Li, B. Lowey, C. Sodroski, S. Krishnamurthy, H. Alao, H. Cha, S. Chiu, R. El-Diwany, M. G. Ghany and T. J. Liang, *Nat. Commun.*, 2017, **8,** 1789.
6. R. C. Lee and V. Ambros, *Science*, 2001, **294**, 862-864.
7. A. Qu, M. Sun, L. Xu, C. Hao, X. Wu, C. Xu, N. A. Kotov and H. Kuang, *Proc. Natl. Acad. Sci. USA*, 2019, **116**, 3391-3400.
8. S. Li, L. Xu, W. Ma, X. Wu, M. Sun, H. Kuang, L. Wang, N. A. Kotov and C. Xu, *J. Am. Chem. Soc.*, 2016, **138**, 306-312.
9. P. Zhang, X. Wu, R. Yuan and Y. Chai, *Anal. Chem.*, 2015, **87**, 3202-3207.
10. C. K. K. Choi, J. Li, K. Wei, Y. J. Xu, L. W. C. Ho, M. Zhu, K. K. W. To, C. H. J. Choi and L. Bian, *J. Am. Chem. Soc.*, 2015, **137,** 7337-7346.
11. T. Xue, S. Yu, X. Zhang, X. Zhang, L. Wang, Q. Bao, C. Chen, W. Zheng and X. Cui, *Sci. Rep.*, 2016, **6**, 21254.
12. D. Rodrigo, O. Limaj, D. Janner, D. Etezadi, F. J. García de Abajo, V. Pruneri and H. Altug, *Science*, 2015, **349**, 165-168.
13. F. Li, H. Pei, L. Wang, J. Lu, J. Gao, B. Jiang, X. Zhao and C. Fan, *Adv. Funct. Mater.*, 2013, **23**, 4140-4148.
14. T. Xue, X. Cui, W. Guan, Q. Wang, C. Liu, H. Wang, K. Qi, D. J. Singh and W. Zheng, *Biosensors Bioelectron.*, 2014, **58**, 374-379.
15. T. Xue, Z. Wang, W. Guan, C. Hou, Z. Shi, W. Zheng and X. Cui, *RSC Advances*, 2014, **4,** 50789-50794.
16. H. Liu, K. Hu, D. Yan, R. Chen, Y. Zou, H. Liu and S. Wang, *Adv. Mater.*, 2018, **30,** 1800295.
17. C. Zhu, Z. Zeng, H. Li, F. Li, C. Fan and H. Zhang, *J. Am. Chem. Soc.*, 2013, **135,** 5998-6001.
18. S. Wang, S. Wei, S. Wang, X. Zhu, C. Lei, Y. Huang, Z. Nie and S. Yao, *Anal. Chem.*, 2019, **91,** 1651-1658.
19. A. Sinha, Dhanjai, H. Zhao, Y. Huang, X. Lu, J. Chen and R. Jain, *TrAC, Trends Anal. Chem.*, 2018, **105,** 424-435.
20. C. C. Mayorga-Martinez, R. Gusmão, Z. Sofer and M. Pumera, *Angew. Chem. Int. Ed.*, 2019, **58,** 134-138.
21. S. Zhang, S. Guo, Z. Chen, Y. Wang, H. Gao, J. Gómez-Herrero, P. Ares, F. Zamora, Z. Zhu and H. Zeng, *Chem. Soc. Rev.*, 2018, **47,** 982-1021.
22. S. Zhang, Z. Yan, Y. Li, Z. Chen and H. Zeng, *Angew. Chem. Int. Ed.*, 2015, **54,** 3112-3115.
23. T. Xue, W. Liang, Y. Li, Y. Sun, Y. Xiang, Y. Zhang, Z. Dai, Y. Duo, L. Wu, K. Qi, B. N. Shivananju, L. Zhang, X. Cui, H. Zhang and Q. Bao, *Nat. Commun.*, 2019, **10,** 28.
24. J. Ji, X. Song, J. Liu, Z. Yan, C. Huo, S. Zhang, M. Su, L. Liao, W. Wang, Z. Ni, Y. Hao and H. Zeng, *Nat. Commun.*, 2016, **7,** 13352.
25. M. Pumera and Z. Sofer, *Adv. Mater.*, 2017, **29,** 1605299.
26. Y. Kadioglu, S. B. Kilic, S. Demirci, O. Ü. Aktürk, E. Aktürk and S. Ciraci, *Phys. Rev. B*, 2017, **96,** 245424.
27. Y. Wang, K. Chen, H. Hao, G. Yu, B. Zeng, H. Wang, F. Zhang, L. Wu, J. Li, S. Xiao, J. He, Y. Zhang and H. Zhang, *Nanoscale*, 2019, **11,** 2637-2643.
28. F. Federspiel, G. Froehlicher, M. Nasilowski, S. Pedetti, A. Mahmood, B. Doudin, S. Park, J.-O. Lee, D. Halley, B. Dubertret, P. Gilliot and S. Berciaud, *Nano Lett.*, 2015, **15,** 1252-1258.
29. J. J. Xu, W. W. Zhao, S. Song, C. Fan and H. Y. Chen, *Chem. Soc. Rev.*, 2014, **43,** 1601-1611.
30. Y. Xu, B. Wang, R. Kaur, M. B. Minameyer, M. Bothe, T. Drewello, D. M. Guldi and M. von Delius, *Angew. Chem.*, 2018, **130,** 11723-11727.
31. F. Reis, G. Li, L. Dudy, M. Bauernfeind, S. Glass, W. Hanke, R. Thomale, J. Schäfer and R. Claessen, *Science*, 2017, **357,** 287-290.
32. M. Zhou, W. Ming, Z. Liu, Z. Wang, P. Li and F. Liu, *Proc. Natl. Acad. Sci. USA*, 2014, **111,** 14378-14381.
33. T. Nagao, J. T. Sadowski, M. Saito, S. Yaginuma, Y. Fujikawa, T. Kogure, T. Ohno, Y. Hasegawa, S. Hasegawa and T. Sakurai, *Phys. Rev. Lett.*, 2004, **93,** 105501.
34. Y. Li, J. Wang, Z. Deng, Y. Wu, X. Sun, D. Yu and P. Yang, *J. Am. Chem. Soc.*, 2001, **123,** 9904-9905.
35. Q. Q. Yang, R. T. Liu, C. Huang, Y. F. Huang, L. F. Gao, B. Sun, Z. P. Huang, L. Zhang, C. X. Hu, Z. Q. Zhang, C. L. Sun, Q. Wang, Y. L. Tang and H. L. Zhang, *Nanoscale*, 2018, **10,** 21106-21115.
36. J. S. Lannin, J. M. Calleja and M. Cardona, *Phys. Rev. B*, 1975, **12,** 585-593.
37. Y. Wang, W. Huang, J. Zhao, H. Huang, C. Wang, F. Zhang, J. Liu, J. Li, M. Zhang and H. Zhang, *J. Mater. Chem. C*, 2019, **7,** 871-878.
38. D. Dini, M. J. F. Calvete and M. Hanack, *Chem. Rev.*, 2016, **116,** 13043-13233.
39. V. Mamidala, L. Polavarapu, J. Balapanuru, K. P. Loh, Q. H. Xu and W. Ji, *Opt. Express*, 2010, **18,** 25928-25935.
40. X. Liao, Q. Wang, H. Ju, *Chem. Commun.*, 2014, **50,** 13604-13607
41. Y. Wu, J. Huang, X. Yang, Y. Yang, K. Quan, N. Xie, J. Li, C. Ma and K. Wang, *Anal. Chem.*, 2017, **89,** 8377-8383.